Solid State Sciences 12 (2010) 795–802

Contents lists available at ScienceDirect

Solid State Sciences

journal homepage: www.elsevier.com/locate/ssscie

Thiazolo[5,4-d]thiazole-2,5-dicarboxylic acid, $C_6H_2N_2O_4S_2$, and its coordination polymers

Alessia Aprea, Valentina Colombo, Simona Galli*, Norberto Masciocchi, Angelo Maspero*, Giovanni Palmisano

Dipartimento di Scienze Chimiche e Ambientali, Università dell'Insubria, via Valleggio 11, I-22100 Como, Italy

ARTICLE INFO

Article history:
Received 17 December 2009
Received in revised form
25 January 2010
Accepted 3 February 2010
Available online 11 February 2010

Keywords:
Coordination polymers
Powder diffraction
Thermal analysis
Crystal structure

ABSTRACT

Thiazolo[5,4-d]thiazole-2,5-dicarboxylic acid, $C_6H_2N_2O_4S_2$, was isolated as a polycrystalline material, and its crystal structure was determined by *ab-initio* X-ray powder diffraction (XRPD) methods. This species, upon deprotonation, was subsequently used in preparing the new coordination polymers $Ag_2(C_6N_2O_4S_2)$, $Mn(C_6N_2O_4S_2)(H_2O)_2$, $Co(C_6N_2O_4S_2)(H_2O)_2$, $Cu(C_6N_2O_4S_2)(H_2O)$ and $Zn(C_6N_2O_4S_2)(H_2O)_2$, fully characterized by analytical, thermal and XRPD structural methods – including *in situ* thermodiffractometry and simultaneous TGA and DSC. In the first-row transition metal derivatives, the $[C_6N_2O_4S_2]^{2-}$ anion systematically prefers the *N,O*-chelating, *vs.* the expected *O,O'*-bridging, coordination mode, not allowing the formation of porous 3D frameworks. Indeed, these species are dense 1D coordination polymers. At variance, the silver derivative possesses a complex, dense 3D framework, due to the presence of μ_6-$[C_6N_2O_4S_2]^{2-}$ ligands showing two μ_2-bridging carboxylates and two monohapto *N*-donor sites. When dehydration is viable, materials of $E_n(C_6N_2O_4S_2)$ formulation are irreversibly recovered ($n = 1$ for E = Mn, Co, Zn, Cu; $n = 2$, for E = H).

1. Introduction

In the last years, coordination polymers and metal-organic frameworks have been widely studied, and the number of new species belonging to these categories has impressively risen [1]. This is largely due to the extreme versatility of their chemistry: simple changes of metal ions, organic ligands, reactants stoichiometry and reaction conditions can lead to compounds differing in metal coordination geometry, framework topology, solvent trapping, thermal stability, polymorphic behavior and overall structural flexibility. Within this large list of chemically and structurally characterized species, some have shown very interesting functional aspects, ranging from catalytic [2], adsorptive [3], magnetic [4] and optical [5], to dielectric [6] and even antimicrobial [7] properties. These results have pushed many groups toward the preparation of novel systems, hopefully benefiting from the introduction of suitably tailored ligands in their crystalline frameworks.

The main structural method for studying these materials is, and will remain, the conventional X-ray single-crystal diffraction technique which, however, must rely on not always available single-crystals of suitable size and quality. To overcome this problem, X-ray powder diffraction (XRPD) methods and suitably designed neutron and synchrotron radiation diffraction techniques have recently found vast diffusion and implementation, disclosing important structural features which would have otherwise remained inaccessible [8].

In the last decade, we have been interested in the rich structural chemistry of functional materials, putting particular emphasis on porous coordination polymers (PCP's) capable to selectively adsorb gases, liquids or ionic pairs under the appropriate conditions [9]. We have thus investigated manifold PCP's in which transition metal ions are bridged by geometrically stiff ligands possessing strong Lewis base capacity and high thermal stability. After having employed aromatic systems bearing negatively charged tetrazolyl [10], pyrazolyl [11] and *N*-aromatic oxo fragments [12], we have driven our attention to a *N,S*-heteroaromatic molecule, the thiazolo[5,4-d]thiazole-2,5-dicarboxylic acid, $C_6H_2N_2O_4S_2$ (**1**, see Scheme 1). Indeed, upon deprotonation, **1** affords the $[C_6N_2O_4S_2]^{2-}$ anion, a polydentate ligand which could behave as a long-spacer between transition metal ions, as recently demonstrated in the case of its alkaline earth coordination polymers [13]. In its bishydrated form, $\mathbf{1}\cdot\mathbf{2H_2O}$, this ligand was initially isolated and studied *per se*, sagaciously combining analytical and structural techniques (TG, DSC, XRPD and

* Corresponding authors. Fax: +39 31 23866230.
E-mail addresses: simona.galli@uninsubria.it (S. Galli), angelo.maspero@uninsubria.it (A. Maspero).

1293-2558/$ – see front matter © 2010 Elsevier Masson SAS. All rights reserved.
doi:10.1016/j.solidstatesciences.2010.02.016

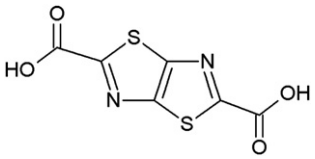

Scheme 1. Molecular connectivity of the $C_6H_2N_2O_4S_2$ species.

thermodiffractometry). Subsequently, **1** was coupled to first- and second-row transition metal ions, aiming at the formation of new PCP's. Of the many metal ions tested, only Ag(I), Mn(II), Co(II), Zn(II) and Cu(II) yielded analytically pure and polycrystalline coordination polymers, *i.e.* $Ag_2(C_6N_2O_4S_2)$, **2**, $Mn(C_6N_2O_4S_2)(H_2O)_2$, **3**, $Co(C_6N_2O_4S_2)(H_2O)_2$, **4**, $Zn(C_6N_2O_4S_2)(H_2O)_2$, **5** and $Cu(C_6N_2O_4S_2)(H_2O)$, **6**. As later shown, none of the prepared materials is adequate for gas adsorption. This behavior has been *ex post* explained by the tendency of the $[C_6N_2O_4S_2]^{2-}$ dianion to coordinate with the *N*,*O*-chelating [14], *vs.* the *O*,*O*′-bridging, mode, the latter being ubiquitous in polycarboxyarene ligands of highly porous, and chemically inert, 3D frameworks [15].

In the following, the preparation and the main structural features of **1** and of its transition metal derivatives **2–6**, derived by the less conventional *ab-initio* powder diffraction technique, are reported and discussed, including an extensive thermodiffractometric characterization.

2. Results and discussion

2.1. Synthesis and spectroscopy

The thiazolo[5,4-d]thiazole-2,5-dicarboxylic acid, **1**, has been reacted with several metallic salts. With the Ag(I), Mn(II), Co(II), Cu(II) and Zn(II) ions, microcrystalline species were isolated [16]. The reaction conditions required by **1** deserve a few comments. Due to its very limited solubility in many common solvents, all the reactions were carried out dissolving it in DMSO. **1** is also known to possess a limited thermal stability, as it may decarboxylate at low temperature [17]; thus, the reaction mixtures were initially kept at only 40 °C. Only at a later stage, *i.e.* after metal complexation occurred, the reaction vessels were heated further. Notably, the intrinsic acidity of the metal ions (assisted, in a few cases, by the presence of acetate groups) allowed ligand deprotonation and coordination polymers formation without the necessity of adding external bases.

The infrared spectra of complexes **3–6** are quite similar: their main features are a broad band at about 3190 cm^{-1}, attributed to the O–H stretching of the water molecules present in the crystal lattices, and a sharp band at about 1673 cm^{-1}, attributed to the C=O stretching of the carboxylate groups; if compared to that found in the free ligand (1746 cm^{-1}), this band is remarkably red shifted, due to the coordination to the metal ions (adopting, as later found by XRPD, a *N*,*O*-chelating mode). In the infrared spectrum of complex **2**, the C=O stretching determines a sharp band at even lower wavenumbers (1612 cm^{-1}), which is consistent with the significantly different ligand coordination mode in the silver derivative with respect to species **3–6** (*vide infra*). In agreement with the analytical and structural results, in the IR of **2** no O–H stretching mode of coordinated or hosted water molecules is observed.

2.2. Crystal structure of $C_6H_2N_2O_4S_2{\cdot}2H_2O$, **1·2H₂O**

The crystal structure of this species, shown in Fig. 1, is monoclinic, $P2_1/c$, and contains $C_6H_2N_2O_4S_2$ moieties (located on inversion centres) and water molecules, interacting with the organic species by evident hydrogen bonds (see caption to Fig. 1). As far as the organic $C_6H_2N_2O_4S_2$ moiety is concerned, the freely refined torsion angle of the carboxylic residue slightly deviates from planarity [6.8(3)°, *syn*-S–C–C–O sequence], thus maintaining a largely delocalized π-system. Hydrogen atoms cannot be detected by XRPD. Yet, given the observed coordination geometry, we propose that the acidic proton on the organic acid resides on the carboxylic oxygen O1; the two hydrogen atoms of the water molecule interact with the remaining basic sites with slightly longer distances. Taking into account the hydrogen bond interactions, the overall connectivity is three-dimensional. Moreover, as expected for thia-aromatic moieties with markedly flat shapes, significant S···S contacts are present (3.42–3.48 Å), which, in similar systems, have been associated with interesting electronic conduction processes [18]. For comparison, the strictly related molecule 2,5-di-2-thienylthiazolo[4,5-*d*]thiazole [19] shows intermolecular S···S contacts of 3.58 Å and a twist of the aromatic rings of 1.69(8)°, comparable to the values found in **1·2H₂O**.

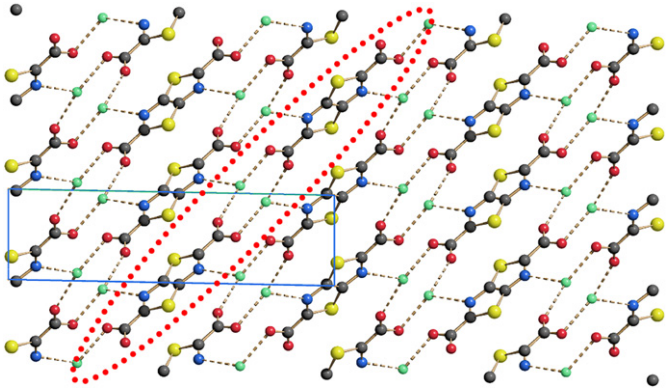

Fig. 1. Crystal structure of $C_6H_2N_2O_4S_2{\cdot}2H_2O$, **1·2H₂O**, viewed down **b**. Horizontal axis, **c**; vertical axis, **a**. Carbon, grey; nitrogen, blue; carboxylic oxygen, red; water oxygen, light green; sulfur, yellow. Hydrogen bonds are drawn as fragmented lines. The red ellipse highlights the molecular ribbons described in the text. Relevant intermolecular distances: Ow···O1 2.58(1), Ow···O2 2.73(1), Ow···N1 3.03(2) Å.

2.3. Crystal structure of $Ag_2(C_6N_2O_4S_2)$, **2**

This species crystallizes in the monoclinic $P2_1/n$ space group. The asymmetric unit features one crystallographically independent Ag(I) ion and half $C_6N_2O_4S_2$ moiety, the whole ligand being located on an inversion centre (see Fig. 2). Each silver ion is coordinated to five different atoms: a rather distorted digonal coordination [Ag–O1 2.241(7) Å, Ag–O2 2.268(6) Å and O1–Ag–O2 135.8(5)°] is completed by three ancillary longer interactions (Ag–N1 2.54 Å, Ag–O2′ 3.04 Å and Ag–S1 2.88 Å). This rich connectivity generates a rather dense three-dimensional polymer, with no cavities capable of hosting water (or other small) molecules. The tendency of Ag(I) ions to afford dense structures with polytopic aza-aromatic systems has already been observed for the Ag_2(btb) species (H_2btb = 1,4-bis(5-tetrazolyl)benzene), in which each metal ion is tetracoordinated and the btb fragment behaves as a rare μ_8-ligand [10]. Whether in the present case a μ_4- or a higher connectivity for the dicarboxylate anion is present, it depends on the distance cut-off set for the long Ag–X interactions. As in **1·2H₂O**, also in **2** the COO^- groups are only slightly rotated off the average molecular plane of the organic ligand, by a mere 1.7(6)° [*syn*-S–C–C–O sequence]. Interestingly, and at variance with **1·2H₂O**, no S···S contacts are present in **2**.

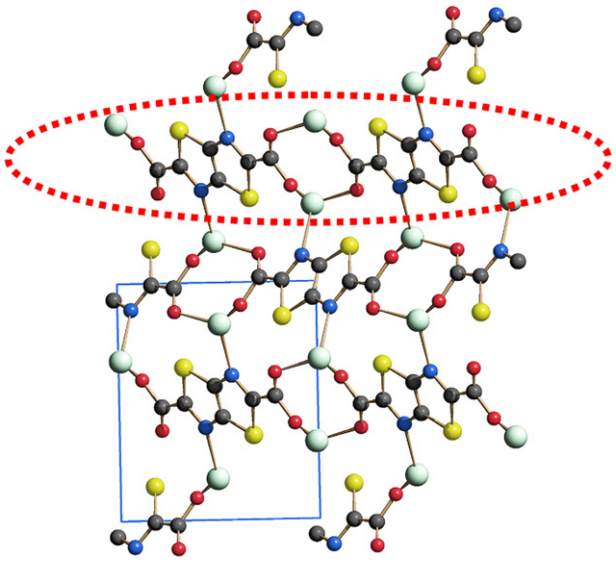

Fig. 2. Crystal structure of $Ag_2(C_6N_2O_4S_2)$, **2**, viewed down **a**. Horizontal axis, **c**; vertical axis, **b**. Carbon, grey; nitrogen, blue; oxygen, red; sulfur, yellow; silver, light grey. The red ellipse highlights the molecular ribbons described in the text. Relevant bond distances: Ag–O1 2.241(7), Ag–O2 2.268(6), Ag–N1 2.539(4) Å.

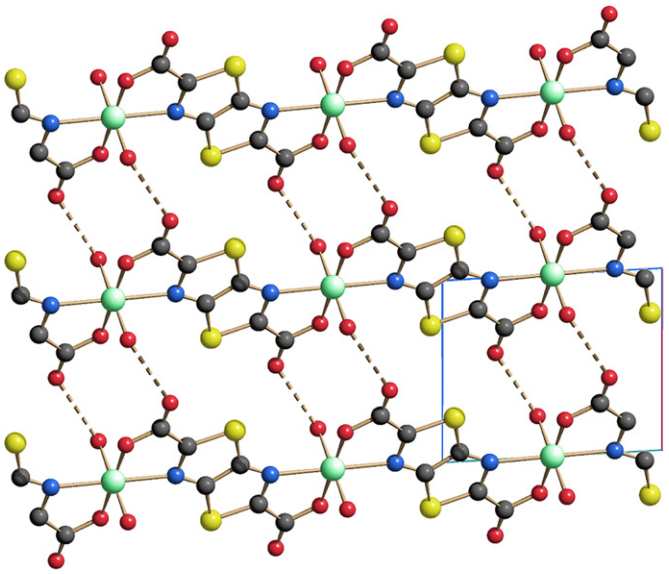

Fig. 4. Crystal structure of $Co(C_6N_2O_4S_2)(H_2O)_2$, **4**, viewed down **a**. Horizontal axis, **c**; vertical axis, **b**. Carbon, grey; nitrogen, blue; oxygen, red; sulfur, yellow; cobalt, light green. Relevant bond distances: Co–O1w 1.89(1), Co–O1 1.88(1), Co–N1 2.182(1) Å. At the drawing resolution, the structure of $Zn(C_6N_2O_4S_2)(H_2O)_2$, **5**, is identical, with Zn–O1w 1.86(1), Zn–O1 1.88(1), Zn–N1 2.192(1) Å.

2.4. Crystal structure of $M(C_6N_2O_4S_2)(H_2O)_2$ ($M = Mn$, **3**; $M = Co$, **4**, $M = Zn$, **5**)

These three species, despite sharing the same molecular formula and space group, belong to two distinct structural classes: the $Z = 1$ one, featuring the strictly isomorphous Co and Zn derivatives, and the $Z = 2$ one, involving the Mn species (*not* isomorphous with **4** and **5**). In **4** and **5**, metal ions and organic ligands lie on inversion centres, while in **3**, every fragment is in general position. There are, however, strong structural similarities: in all three phases, the M(II) ions are octahedrally coordinated, due to the presence of two *N*,*O*-chelating rings (from different $[C_6N_2O_4S]^{2-}$ ligands) and of two axial water molecules, completing the MN_2O_4 coordination sphere. As shown in Figs. 3 and 4, such a coordination generates infinite 1D ribbons elongating along **b** (in **3**) or **c** (in **4** and **5**), pseudohexagonally packed (as expected for rods of elliptical or nearly circular cross section [20]), and interacting by hydrogen bond contacts involving water molecules and carboxylate residues.

One question arises: what is the crystallochemical reason for imposing, in **3**, a different crystal structure than in **4** and **5**? A visual inspection of the local geometry and of the crystal packing does not immediately answer this question; also the overall connectivity within the crystal, determined by the extended network of hydrogen bonds, appears undistinguishable. However, the *only well defined geometrical parameters*, the intermetallic M···M distances, show some significant differences (i) along the 1D chains (8.13 Å in **3** *vs.* 7.90 Å in **5** − **4** being very similar to **5**); (ii) across adjacent chains (5.13 and 6.43 Å in **3** *vs.* 5.20 and 6.56 Å in **5**), as if a partial sliding of parallel chains occurred. Considering that Shannon octahedral crystal radii [21] for Zn(II), high-spin Co(II) and Mn(II) ions are 0.88, 0.88 and 0.97 Å, respectively, we tentatively suggest that the different features are driven by the size of the metal ions, *i.e.*, ultimately, by the metal-to-ligand distances, which XRPD alone cannot assess with the sought accuracy. Finally, the $-a$, $-\frac{1}{2}c$, $-b$ transformation of the unit cell of **3** generates a triclinic lattice ($a = 5.134$, $b = 6.736$, $c = 8.134$ Å, $\alpha = 82.67$, $\beta = 74.26$, $\gamma = 84.57°$) vaguely similar to, but significantly different from, those of **4** and **5**, thus furthermore proving that **3** is not isomorphous with the Co(II) and Zn(II) species.

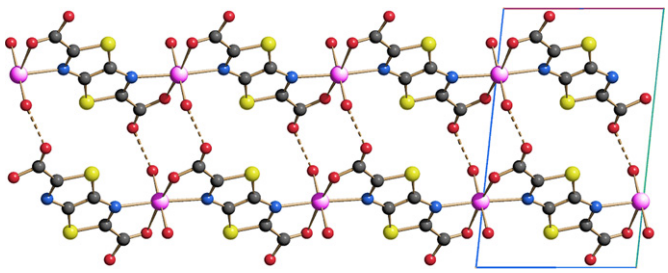

Fig. 3. Crystal structure of $Mn(C_6N_2O_4S_2)(H_2O)_2$, **3**, viewed down **a**. Horizontal axis, **b**; vertical axis, **c**. Carbon, grey; nitrogen, blue; oxygen, red; sulfur, yellow; manganese, purple. Relevant bond distances: Mn–O1w 2.01(3), Mn–O2w 2.02(3), Mn–O2 2.09(2), Mn–O4 2.33(2), Mn–N1 2.27(2), Mn–N2 2.34(2) Å.

2.5. Crystal structure of $Cu(C_6N_2O_4S_2)(H_2O)$, **6**

The crystal structure of this species, shown in Fig. 5, is monoclinic, *C2/c*, and contains Cu(II) ions and $C_6N_2O_4S_2$ moieties both located on inversion centres. Differently from the derivatives discussed above, *a single* water molecule, lying on a twofold axis, is present *per* formula unit. The Cu–O1 and Cu–N1 distances, defining the equatorial plane of a heavily Jahn–Teller-elongated octahedral coordination, are 1.87 and 1.91 Å (O1–Cu–N1 angle of 88.2°), while the axial water molecules are found at a rather distant position (Cu···O1w 2.80 Å), bridging two different Cu(II) ions (Cu···O1w··· Cu 113.4°). This unexpected coordination mode closely matches that found in the hydrated $Cu(pz)_2$ (Hpz = pyrazole) phase [9b], and is apparently stabilized, in the latter as well as in species **6**, by well defined *inter*molecular contacts (OH···π_{pz} in $Cu(pz)_2 \cdot H_2O$ [22], and OH···O in **6**). The different stoichiometry adopted by the copper complex (a monohydrated species *vs.* the bishydrated **3**–**5** ones) thus finds a stereochemical explanation, driven mostly by the specific electronic requirements of the d^9 ion.

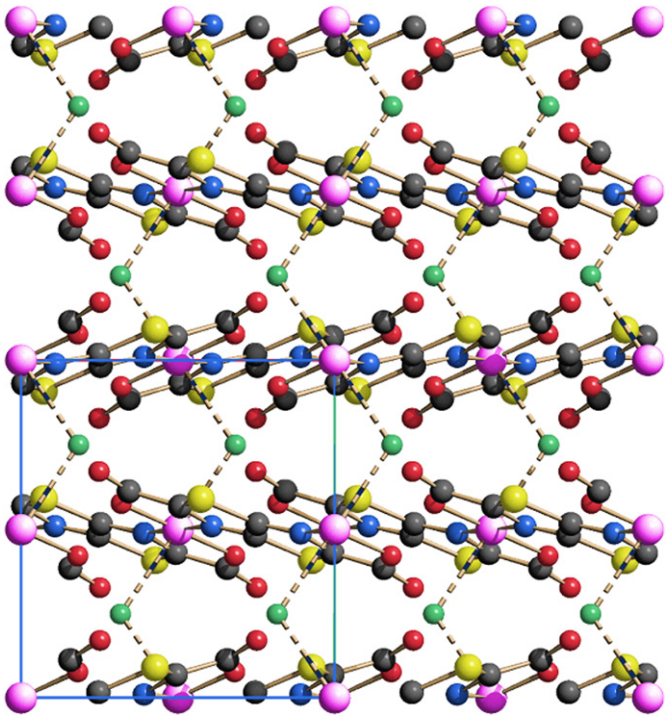

Fig. 5. Crystal structure of $Cu(C_6N_2O_4S_2)(H_2O)_2$, **6**, viewed down **a**. Horizontal axis, **b**; vertical axis, **c**. Carbon, grey; nitrogen, blue; carboxylate oxygen, red; water oxygen, light green; sulfur, yellow; copper, purple. Relevant bond distances: Cu–O1 1.87(1), Cu–N1 1.88(1), Cu–N1 1.915(2) Å, Cu···O1w 2.80(1), O1w···O2 2–83(2) Å.

2.6. Comparative structural analysis

The crystal and molecular structures derived from our powder diffraction measurements are of much less quality than those obtainable from conventional single-crystal data, and the Independent Atom Model could not be used. Instead, rigid bodies, flexible at the Ar–CO_2 torsions, were employed (see Experimental section), granting significance of the refined parameters, and convergence to chemical plausible models. As an obvious consequence, a meaningful structural discussion needs to avoid subtle (inaccessible) geometrical details, focussing on supramolecular, rather than molecular, features.

In **1·2H₂O**, six atoms are involved in hydrogen bonding with lattice water molecules. Ribbons of OH···O hydrogen bonded molecules generate a 1D polymer, linked to neighboring ribbons by ancillary (and weaker) Ow···N interactions. This structural feature is maintained in **2**, once allowance is made for substituting the water molecules and the acidic protons in **1·2H₂O** (*i.e.*, "H_3O^+ fragments") with nearly isosteric Ag(I) ions. Figs. 1 and 2 further highlight, in the red ellipses, this analogy. This similarity is, however, not maintained in the long range, since the two structures are not isomorphous.

This supramolecular stability of **1·2H₂O**, disrupted upon thermally-induced dehydration, is further complemented by intermolecular S···S contacts of the attractive type (3.42–3.48 Å, *vide supra*). These intermolecular contacts are definitely absent in **2** and **6**, but of comparable nature in **3**, **4** and **5** (3.51, 3.41 and 3.38 Å, respectively).

Within each ligand, the twists of the carboxylic residues out from the average heteroaromatic planes range from a mere 0.9° and 0.7° (as measured by the *syn*-S–C–C–O sequence) for the isomorphous couple **4** and **5**, up to 17.5° in **3**. Overall, this trend manifests the stability of π-conjugation, as well as the nearly planar conformation of the chelating N–C–C–O bite (where pertinent).

2.7. Thermal analyses

The following thermoanalytical results have been obtained by coupling conventional thermal analyses (simultaneous TG and DSC) with thermodiffractometric measurements, assessing the nature of the products generated by progressive heating. Table 1 contains the most relevant thermal features derived from our combined thermal analyses. All TG and DSC traces, the complete thermodiffractograms, as well as the relative changes of unit cell parameters as a function of temperature, are supplied in the Supplementary information.

Upon heating, species **1·2H₂O**, $C_6H_2N_2O_4S_2\cdot 2H_2O$, undergoes an endothermic event ($\Delta H = 91.3$ kJ mol^{-1}; onset at 77 °C), accompanied by a weight loss of *ca.* 11.8%, attributed to the evacuation of the clathrated water molecules (calculated mass loss 13.5%). Once formed, the anhydrous species **1** is stable up to 195 °C, where sublimation begins ($\Delta H = 82.7$ kJ mol^{-1}). *In situ* thermodiffractometric measurements allowed to assess that the high crystallinity of **1·2H₂O** is lost in the 70–90 °C range. The only remarkable feature of the nearly amorphous-like XRPD traces of **1** collected in the 90–170 °C range is a broad peak with $d = 3.25$ Å (Fig. 6). The latter

Table 1
TG/DSC and TXRPD–derived results for compounds $C_6H_2N_2O_4S_2\cdot 2H_2O$, **1·2H₂O**, $Ag_2(C_6N_2O_4S_2)$, **2**, $Mn(C_6N_2O_4S_2)(H_2O)_2$, **3**, $Co(C_6N_2O_4S_2)(H_2O)_2$, **4**, $Zn(C_6N_2O_4S_2)(H_2O)_2$, **5**, and $Cu(C_6N_2O_4S_2)(H_2O)$, **6**.

Compound	$C_6H_2N_2O_4S_2\cdot 2H_2O$ (**1·2H₂O**)	$Ag_2(C_6N_2O_4S_2)$ (**2**)	$Mn(C_6N_2O_4S_2)(H_2O)_2$ (**3**)	$Co(C_6N_2O_4S_2)(H_2O)_2$ (**4**)	$Zn(C_6N_2O_4S_2)(H_2O)_2$ (**5**)	$Cu(C_6N_2O_4S_2)(H_2O)$ (**6**)
First Event	Dehydration	Decarboxylation	Dehydration	Dehydration	Dehydration	Dehydration + Decarboxylation
T_{onset}, °C	76	220	150	170	140	180
Exp. mass loss	11.8 %	19.3 %	11.1 %	11.7 %	11.4 %	31.4 %
ΔH, kJ mol^{-1}	91	−82	111	91	80	−41
Crystal system	Monoclinic	Monoclinic	Triclinic	Triclinic	Triclinic	Monoclinic
$\partial lna/\partial T$, 10^{-6} K^{-1}	–[a]	17	58	46	14[b]	6[c]
$\partial lnb/\partial T$, 10^{-6} K^{-1}	–	37	11	29	−5[b]	8[c]
$\partial lnc/\partial T$, 10^{-6} K^{-1}	–	45	59	4	−13[b]	60[c]
$\partial lnV/\partial T$, 10^{-6} K^{-1}	–	83	113	102	21[b]	67[c]

[a] Dehydration occurs at a too low temperature to allow the determination of reliable thermal expansion coefficients.
[b] The quality of the TXRPD data did not allow the refinement of the specimen height displacement error. Accordingly, the thermal expansion coefficients derived for **5**, which should be similar to those of the isomorphous species **4**, may contain unavoidable systematic errors. However, the trend observed in **4** and **5** is similar, once correction for a (purely phenomenological) approximate 20×10^{-6} value is applied to the $\partial lnp_i/\partial T$ coefficients, (p_i are the *a*, *b*, *c* lattice constants).
[c] In calculating the thermal expansion coefficients, the curvature of the plot of the cell parameters vs. temperature (shown in the Supporting Information) has been neglected by taking only the low temperature range.

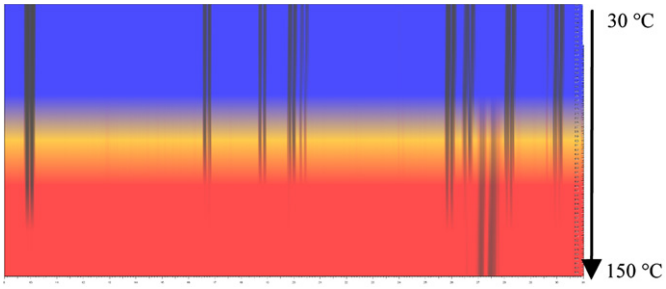

Fig. 6. X-ray powder thermodiffactogram of species $C_6H_2N_2O_4S_2{\cdot}2H_2O$, **1·2H₂O**. The complete loss of crystallinity is already evident at 90 °C.

value suggests that, in **1**, the molecules adopt a flat conformation with only a (partial) stacking order of the aromatic moieties, with no detectable lateral periodicity.

Compound **2**, $Ag_2(C_6N_2O_4S_2)$, not containing solvent molecules, is stable up to about 220 °C, where an abrupt exothermic event ($\Delta H = -82$ kJ mol^{-1}), accompanied by a mass change of 19.3%, takes place. The product recovered at 300 °C is amorphous and is likely the result of decarboxylation (calculated mass loss 19.8%). Decomposition continues with a further, slow and continuous, mass loss starting at about 480 °C and eventually yielding an amorphous material. TXRPD measurements indicated a linear increase of the all the cell parameters as a function of temperature up to decomposition. The increase is reasonably due to thermal expansion, and confirms the dense nature of this system.

Compound **3**, $Mn(C_6N_2O_4S_2)(H_2O)_2$, is stable to about 150 °C, where water elimination begins ($\Delta H = 111$ kJ mol^{-1}; observed mass loss 11.1%), to yield an amorphous material (TXRPD evidence). Decomposition takes place through a structured series of exothermic events starting at about 280 °C and results in an amorphous material. Disregarding as a first approximation that **3** is monoclinic, before dehydration the variation of *b*, the chains elongation direction, is minimal; larger modifications occur perpendicular to it, where much softer intermolecular contacts are at work.

Compound **4**, $Co(C_6N_2O_4S_2)(H_2O)_2$, is stable to about 170 °C, where water elimination begins ($\Delta H = 91$ kJ mol^{-1}; observed mass loss 11.7%), to yield a poorly crystalline species, the metrics of which could not be retrieved. Decomposition begins at 240 °C and yields, through a structured series of exothermic events, an amorphous residue. Disregarding as a first approximation that **4** is triclinic, before dehydration the unit cell experiences a nearly null variation along *c*, the chains elongation direction.

As expected, compound **5**, $Zn(C_6N_2O_4S_2)(H_2O)_2$, shows thermal events similar to those of the isomorphous species **4**. Water elimination begins near 140 °C ($\Delta H = 80$ kJ mol^{-1}; observed mass loss 11.4%), to yield a poorly crystalline species, with an XRPD trace similar to that of the species recovered after dehydration of **4**. Disregarding as a first approximation that **4** is triclinic, and with the caveats put forward at the bottom of Table 1, also **5**, like **4**, shows the minimal cell expansion along *c*, the chain elongation direction. Decomposition induces a structured series of exothermic events starting at about 200 °C to give an amorphous residue.

Finally, compound **6**, $Cu(C_6N_2O_4S_2)(H_2O)$, does not undergo thermal events before 180 °C, temperature at which an endothermic event with a mass loss of *ca.* 31.4% starts. We tentatively interpret this mass loss as simultaneous dehydration and decarboxylation. That easy decarboxylation occurs *only* for species **2** and **6** can be further explained by the relatively high oxidizing power of Ag(I) and Cu(II) ions (and not of Mn, Co and Zn dications), allowing to break the Ar–CO_2 bonds upon heating.

Decomposition then proceeds with a slow and continuous mass loss. No trace of water loss at lower temperatures than 180 °C can be detected, as further proved by our XRPD tests (see Experimental section). This unexpected behavior, however, is not new, as it has already been observed for the hydrated $[Cu(Hoxonic)(H_2O)]_n$ (H_3oxonic = 4,6-dihydroxy-1,3,5-triazine-2-carboxylic acid) polymer [23]. The significant anisotropy of the thermal expansion coefficients (see Table 1) indicates that the polymeric chains adopt, on heating, a larger separation along *c*, *i.e.* along the direction (vertical in Fig. 6) defined by the Cu···Ow···Cu interactions, probably due to the mobility of the water molecules, higher than that of metal-organic fragments.

3. Experimental section

3.1. Materials and methods

All metallic salts and solvents were used as supplied (Aldrich Chemical Co.). $C_6H_2N_2O_4S_2$, **1**, was prepared following literature methods [17]. FT-IR spectra were recorded on a Shimadzu Prestige-21 instrument. Simultaneous TG and DSC analyses were performed in a N_2 stream on a Netzsch STA 409 PC Luxx apparatus (heating rate: 10 °C min^{-1}). Elemental analyses were carried out on a Perkin Elmer CHN Analyzer 2400 Series II.

3.2. Synthesis of $Ag_2(C_6N_2O_4S_2)$, **2**

To a solution of thiazolo[5,4-d]thiazole-2,5-dicarboxylic acid (100 mg, 0.435 mmol) in DMSO (3 mL) a solution of $AgNO_3$ (162.58 mg, 0.957 mmol) in H_2O (3 mL) was added; a white precipitate rapidly formed. This mixture was heated, under continuous stirring, to 40 °C for 1 h; upon heating the vessel to 60 °C and keeping it, always under stirring, for 2 h, the precipitate turned yellow. Finally, the temperature was raised to 90 °C and the mixture was kept at this temperature for 1 h. After slow cooling down to room temperature, the yellow precipitate was filtered, washed with DMSO and H_2O and dried under vacuum to afford the desired product **2** (Yield: 82%). IR (nujol): $\nu = 1613$ (s), 1356 (s), 1288 (m), 1125 (m), 793 (m) cm^{-1}. $Ag_2(C_6N_2O_4S_2)$ (443.9): calcd. C 16.22, N 6.31; found: C 16.20, H 0.17, N 5.66.

3.3. Synthesis of $Mn(C_6N_2O_4S_2)(H_2O)_2$, **3**

To a solution of thiazolo[5,4-d]thiazole-2,5-dicarboxylic acid (100 mg, 0.435 mmol) in DMSO (3 mL), warmed to 40 °C, a solution of $Mn(CH_3COO)_2{\cdot}3H_2O$ (106.60 mg, 0.435 mmol) in H_2O (3 mL) was added and a white precipitate formed. The mixture was kept under stirring for 4 h and then was heated to 100 °C. After the mixture was cooled down to room temperature, the white precipitate was filtered, washed with DMSO and H_2O and dried under vacuum to afford the desired product **3** (Yield: 75%). IR (nujol): $\nu = 3185$ (br), 1673 (s), 1364 (s), 1281 (w), 1146 (m) cm^{-1}. $Mn(C_6N_2O_4S_2)(H_2O)_2$ (319.18): calcd. C 22.56, H 1.25, N 8.77; found: C 22.66, H 1.34, N 8.31.

3.4. Synthesis of $Co(C_6N_2O_4S_2)(H_2O)_2$, **4**

To a solution of thiazolo[5,4-d]thiazole-2,5-dicarboxylic acid (100 mg, 0.435 mmol) in DMSO (3 mL), warmed to 40 °C, a solution of $Co(NO_3)_2{\cdot}6H_2O$ (126.60 mg, 0.435 mmol) in H_2O (3 mL) was added and a pink precipitate formed. The mixture was kept under stirring for 4 h and then was heated to 100 °C. After the mixture was cooled down to room temperature, the pink precipitate was filtered, washed with DMSO and H_2O and dried under vacuum to afford the desired product **4** (Yield: 66%). IR (nujol): $\nu = 3202$ (br),

1665 (s), 1343 (s), 1302 (w), 1146 (m) cm^{-1}. $Co(C_6N_2O_4S_2)(H_2O)_2$ (323.10): calcd. C 22.30, H 1.24, N 8.70; found: C 22.14, H 1.53, N 7.85.

3.5. Synthesis of $Zn(C_6N_2O_4S_2)(H_2O)_2$, **5**

To a solution of thiazolo[5,4-d]thiazole-2,5-dicarboxylic acid (100 mg, 0.435 mmol) in DMSO (3 mL), warmed to 40 °C, a suspension of $Zn(CH_3COO)_2{\cdot}2H_2O$ (95.50 mg, 0.435 mmol) in CH_3CN (3 mL) was added and a white precipitate formed. The mixture was kept under stirring for 3 h and then was heated to 100 °C. After the mixture was cooled down to room temperature, the white precipitate was filtered, washed with DMSO and H_2O and dried under vacuum to afford the desired product **5** (Yield: 60%). IR (nujol): $\nu = 3190$ (br), 1674 (s), 1366 (s), 1288 (w), 1147 (m) cm^{-1}. $Zn(C_6N_2O_4S_2)(H_2O)_2$ (329.63): calcd. C 21.84, H 1.21, N 8.49; found: C 21.41, H 1.56, N 7.71.

3.6. Synthesis of $Cu(C_6N_2O_4S_2)(H_2O)$, **6**

To a solution of thiazolo[5,4-d]thiazole-2,5-dicarboxylic acid (100 mg, 0.435 mmol) in DMSO (3 mL), warmed to 40 °C, a solution of $Cu(ClO_4)_2$ (161.18 mg, 0.435 mmol) in H_2O (3 mL) was added and a blue precipitate formed. The mixture was kept under stirring for 4 h and then was heated to 100 °C. After the mixture was cooled down to room temperature, the cyan precipitate was filtered, washed with DMSO and H_2O and dried under vacuum to afford the desired product **6** (Yield: 63%). IR (nujol): $\nu = 3437$ (m), 3387 (m), 1659 (s), 1323 (s), 1275 (w), 1165 (s), 825 (m), 736 (w) cm^{-1}. $Cu(C_6N_2O_4S_2)(H_2O)$ (309.55): calcd. C 23.26, H 0.65, N 9.05; found: C 23.08, H 0.81, N 8.10.

3.7. X-ray powder diffraction characterization of **1–6**

Polycrystalline samples of the investigated phases were manually ground in an agate mortar and then deposited in the hollow of an aluminium holder equipped with a quartz monocrystal zero background plate. All the diffraction data (CuK_α, 1.5418 Å) were collected on a $\theta{:}\theta$ Bruker Axs D8 Advance vertical scan diffractometer; the generator was operated at 40 kV and 40 mA. The diffractometer was equipped with a Ni filter and a linear Position Sensitive Detector (PSD), with the following optics: primary and secondary Soller slits, 2.3 and 2.5°, respectively; divergence slit, 0.3°; receiving slit, 8 mm. The nominal resolution for the present set-up is 0.08° 2θ (FWHM of the α_1 component) for the LaB_6 peak at about 21.3° (2θ). When indexing seemed viable, overnight scans were performed in the 5–105° 2θ range, with $\Delta 2\theta = 0.02°$. Indexing was performed in all cases with the aid of the single value decomposition approach [24], as implemented in the TOPAS-R suite of programs [25]. Space groups were assigned on the basis of the systematic extinction conditions and confirmed by successful structure solutions and refinements. Structure solutions were performed by using the simulated annealing technique [26] implemented in TOPAS-R, with the organic moieties treated as rigid bodies, derived from the known single-crystal structure of the diethylester of the title compound [27], and, where pertinent, metal atoms and "freely floating" water molecules. The final refinements were performed by the Rietveld method using TOPAS-R, freeing the torsional angles of the C–CO_2 residues. Peak shapes were described by the fundamental parameters approach [28]. The experimental background was fit by a polynomial description. Systematic errors were modelled with sample-displacement angular shifts corrections and with a correction of the preferred orientation in the March–Dollase formulation [29], along the [001], [110], [010] and [001] poles, for species **1·2H₂O**, **2**, **5** and **6**, respectively. Metal atoms were given a refinable, isotropic displacement parameter (B_M), while lighter atoms were assigned a common $B = B_M + 2.0$ Å^2 value. Scattering factors, corrected for real and imaginary anomalous dispersion terms, were taken from the internal library of TOPAS-R. Final R_p, R_{wp}, R_{Bragg} and details on data collections and analyses can be found in Table 2. Fig. 7 shows the final Rietveld refinement plots for species **1·2H₂O-6**.

The definition of the final structural model for species **6** deserves a special comment: while analytical and spectroscopic data

Table 2
Crystal data and refinement details for compounds $C_6H_2N_2O_4S_2{\cdot}2H_2O$, **1·2H₂O**, $Ag_2(C_6N_2O_4S_2)$, **2**, $Mn(C_6N_2O_4S_2)(H_2O)_2$, **3**, $Co(C_6N_2O_4S_2)(H_2O)_2$, **4**, $Zn(C_6N_2O_4S_2)(H_2O)_2$, **5**, and $Cu(C_6N_2O_4S_2)(H_2O)$, **6**.

Compound	$C_6H_2N_2O_4S_2{\cdot}2H_2O$ (**1**·$2H_2O$)	$Ag_2(C_6N_2O_4S_2)$ (**2**)	$Mn(C_6N_2O_4S_2)(H_2O)_2$ (**3**)	$Co(C_6N_2O_4S_2)(H_2O)_2$ (**4**)	$Zn(C_6N_2O_4S_2)(H_2O)_2$ (**5**)	$Cu(C_6N_2O_4S_2)(H_2O)$ (**6**)
Emp. Form.	$C_6H_6N_2O_6S_2$	$C_6Ag_2N_2O_4S_2$	$C_6H_4MnN_2O_6S_2$	$C_6H_4CoN_2O_6S_2$	$C_6H_4N_2O_6S_2Zn$	$C_6H_2CuN_2O_5S_2$
fw, g mol^{-1}	266.26	443.9	319.18	323.10	329.63	309.55
Crystal system	Monoclinic	Monoclinic	Triclinic	Triclinic	Triclinic	Monoclinic
SPGR, *Z*	$P2_1/c$, 2	$P2_1/n$, 2	P-1, 2	P-1, 1	P-1, 1	C2/c, 4
a, Å	4.9518(2)	8.0507 (2)	5.1337(3)	5.2058(4)	5.2050(5)	12.068(1)
b, Å	5.6881(2)	9.4427(3)	8.1344(4)	6.5300(6)	6.5632(6)	8.376(1)
c, Å	17.8636(5)	5.5892(2)	12.7512(7)	7.9678(5)	7.8955(6)	9.366(1)
α, °	90	90	82.670(4)	88.589(6)	89.283(8)	90
β, °	91.093(2)	99.550(2)	84.566(2)	74.206(4)	74.282(7)	74.82(1)
γ, °	90	90	74.257(3)	73.540(4)	72.944(5)	90
V, Å^3	494.22(3)	419.00(2)	507.32(5)	246.42(3)	247.56(4)	913.7(2)
ρ_{calc}, g cm^{-3}	1.789	3.518	2.097	2.188	2.210	2.259
F(000)	260	404	306	155	158	588
Method	Powder	Powder	Powder	Powder	Powder	Powder
λ, Å	Cu-K_α, 1.5418	Cu-K_α, 1.5418	Cu-K_α, 1.5418	Cu-K_α, 1.5418	Cu-K_α, 1.5418	Cu-K_α, 1.5418
μ, cm^{-1}	49.3	411.2	146.6	180.2	73.9	75.2
Diffractometer	Bruker AXS D8 Advance	Bruker AXS D8 Advance	Bruker AXS D8 Advance	Bruker AXS D8 Advance	Bruker AXS D8 Advance	Bruker AXS D8 Advance
T, K	298(2)	298(2)	298(2)	298(2)	298(2)	298(2)
2θ range, °	9–105	14–105	10–105	10–105	10–105	10–105
N_{data}	4801	4551	4751	4751	4751	4751
R_{wp}, R_p	0.128, 0.094	0.085, 0.061 0.063	0.036, 0.023	0.011, 0.007	0.121, 0.093	0.051, 0.032
R_{Bragg}[a]	0.048		0.029	0.010	0.054	0.042

[a] For the less conventional powder diffraction data analysis, the agreement factors are defined by: $R_p = \Sigma_i |y_{i,o} - y_{i,c}|/\Sigma_i |y_{i,o}|$; $R_{wp} = [\Sigma_i w_i (y_{i,o} - y_{i,c})^2/\Sigma_i w_i (y_{i,o})^2]^{1/2}$; $R_B = \Sigma_n |I_{n,o} - I_{n,c}|/\Sigma_n I_{n,o}$; $\chi^2 = \Sigma_i w_i (y_{i,o} - y_{i,c})^2/(N_{obs} - N_{par})$, where $y_{i,o}$ and $y_{i,c}$ are the observed and calculated profile intensities, respectively, while $I_{n,o}$ and $I_{n,c}$ the observed and calculated intensities. The summations run over *i* data points or *n* independent reflections. Statistical weights w_i are normally taken as $1/y_{i,o}$.

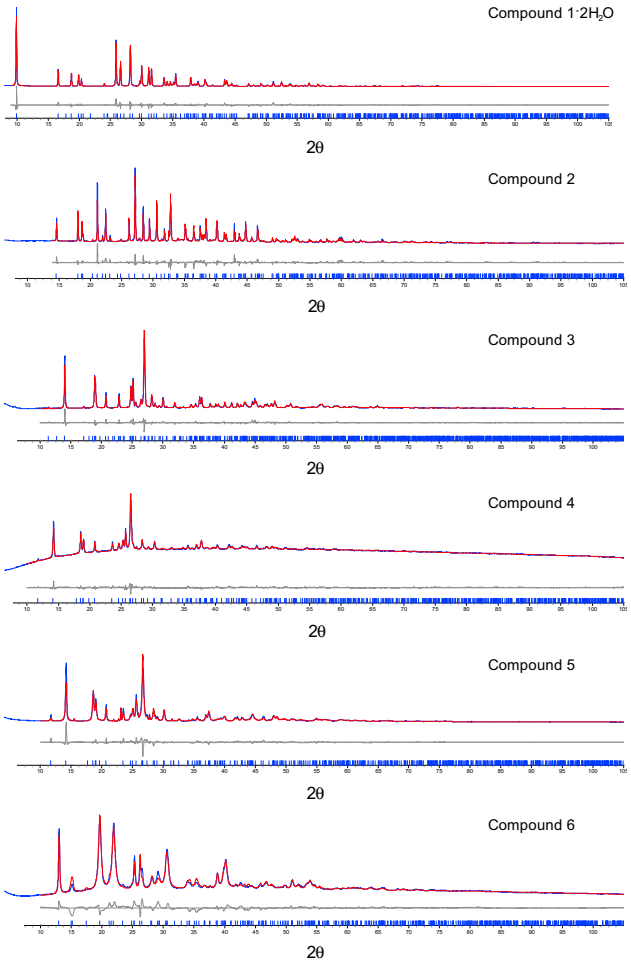

Fig. 7. Top to bottom: Rietveld refinement plots for species **1·2H$_2$O**-**6**. Experimental, calculated and difference plots are depicted in blue, red and grey, respectively. Peak markers are reported at the bottom of each XRPD profile.

coherently suggested the presence of water in the crystal lattice, thermogravimetric analysis did not show any significant mass loss below 200 °C, which was initially taken as a puzzling experimental evidence. Repeated XRPD and TG measurements confirmed the stability of **6** at ambient temperature and the absence of easy water elimination, respectively. Rietveld refinement was also performed on a waterless model, where square-planar (likely reddish) Cu(II) ions are present (in contrast with the observed blue colour): upon omitting the water oxygen atom, disagreement factors rose from 0.051 to 0.088 for R_{wp}, and from 0.042 to 0.100 for R_{Bragg}, thus confirming the presence of the water molecule in the crystal lattice. Crystallographic data for the structural analyses have been deposited with the Cambridge Crystallographic Data Centre, CCDC No. 752907–752912. Copies of this information may be obtained free of charge on application to CCDC, 12 Union Road, Cambridge CB2 1EZ, UK (fax: 44 1223 336 033; e-mail: deposit@ccdc.cam.ac.uk or www: http://www.ccdc.cam.ac.uk).

3.8. Thermodiffractometric analysis

A series of experiments were performed in order to assess the thermal behaviour of the hydrated species, by employing a custom-made sample heater (supplied by Officina Elettrotecnica di Tenno, Italy), mounted on the Bruker AXS Advance D8 diffractometer. The compounds were manually ground in an agate mortar, then deposited in the hollow of an aluminium sample-holder. Typically, the thermodiffractometric experiment was planned on the basis of the STA results: a sequence of scans, in the most significant (low angle) 2θ range, was performed heating *in situ* from room temperature up to the temperature at which loss of crystallinity was complete. The pertinent plots are supplied in the Electronic Supporting information. Le Bail treatment of the acquired data, when viable, allowed to depict the unit cell parameters variations as a function of the temperature (Supporting information) and to derive the corresponding linear thermal expansion coefficients (Table 1). Finally, in comparing the STA and TXRPD results, the reader must be aware that the thermocouple of the TXRPD set-up is *not* in direct contact with the sample, this determining a slight difference in the temperature at which the same event is detected by the two techniques. The STA temperatures have to be considered as more reliable.

4. Conclusions

The already known, but structurally uncharacterized, thiazolo[5,4-d]thiazole-2,5-dicarboxylic acid, $C_6H_2N_2O_4S_2$, was isolated as a highly crystalline, powdered, bishydrated phase. *Ab-initio* X-ray powder diffraction methods were employed in order to assess its crystal structure, as well as those of coordination complexes precipitated on reacting it with different transition metal salts. It was shown that, in all cases studied here [14], the aromatic nitrogen atoms are systematically involved in coordination to the metal ions, preferably through *N,O*-chelation assisted by the neighboring carboxylic ends [30]. Accordingly, the long-spacer nature of this system, mimicking the fashionable terephthalate ligand and its congeners, did not show up, thus limiting the power of this ligand in generating, as originally hoped, porous 3D frameworks.

Aiming at extending the variety of polycrystalline coordination polymers of the title ligand with other metals (in particular, with oxophylic centres like Al), we will further pursue the preparation of new species, testing new synthetic procedures for the still missing members of this family. Moreover, parallel work can be anticipated in the direction of substituting the carboxylate residues with 4-pyrazolato ones, which, through their exo-bidentate coordination mode, may overcome the tendency of using the inner nitrogen atoms in coordination.

The presence of short S···S contacts in **1·2H$_2$O** (and, perhaps, also in **1**), as well as the short stacking sequence of electron rich polyaromatic rings, may impart interesting (semi)conducting properties to these organic materials; aiming to assess this functional aspect, we plan to perform dielectric measurements on pellets of (highly pressed) powdered batches, determining their (di)electrical behaviour under different AC frequency and T regimes. Finally, the presence of magnetically active transition metal ions, bridged within 1D chains, may result in cooperative magnetic effects, with quenching or enhancement of their low temperature magnetic susceptibility [4,31].

Acknowledgments

We thank the Fondazione CARIPLO (Project 2007-5117) for financial support and the Stazione Sperimentale della Seta, Como, for the generous hospitality and use of equipment.

Appendix. Supplementary material

Supporting Information. Thermoanalytical and thermodiffractometric traces, graphical representation of the cell parameters variation as a function of temperature, and CIF files for species **1·2H$_2$O**, **2**–**6**.

Supplementary material associated with this article can be found, in the online version, at doi:10.1016/j.solidstatesciences.2010.02.016.

References

[1] J.R. Long, O.M. Yaghi, Chem. Soc. Rev. 238 (2009) 1213–1214.
[2] See for example A.M. Shultz, O.K. Farha, J.T. Hupp, S.T. Nguyen. J. Am. Chem. Soc. 131 (2009) 4204–4205;
J.Y. Lee, O.K. Farha, J. Roberts, K.A. Scheidt, S.T. Nguyen, J.T. Hupp, Chem. Soc. Rev. 38 (2009) 1450–1459 and references therein.
[3] J.-R. Li, R.J. Kuppler, H.-C. Zhou, Chem. Soc. Rev. 38 (2009) 1477–1504 and references therein.
[4] J.S. Miller, M. Drillon (Eds.), Magnetism: Molecules to Materials, vol. 3, Wiley-VCH, Weinheim, 2002.
[5] Y.-T. Wang, H.-H. Fan, H.-Z. Wang, X.-M. Chen, Inorg. Chem. 44 (2005) 4148–4150; S. Galli, N. Masciocchi, E. Cariati, A. Sironi, E. Barea, M.A. Haj, J.A.R. Navarro, J.M. Salas, Chem. Mater. 17 (2005) 4815–4824.
[6] See for example J. Banys, M. Kinka, G. Völkel, W. Böhlmann, A. Pöppl. Appl. Phys. A 96 (2009) 537–541 and references therein.
[7] See for example R. Rowan, T. Tallon, A.M. Sheahan, R. Curran, M. McCann, K. Kavanagh, M. Devereux, V. McKee. Polyhedron 25 (2005) 1771–1778 and references therein.
[8] W.I.F. David, K. Shankland, L.B. McCusker, Ch. Baerlocher (Eds.), Structure Determination from Powder Diffraction Data (IUCr Monographs on Crystallography), Oxford Univerity Press, Oxford, UK, 2002.
[9] E. Barea, J.A.R. Navarro, J.M. Salas, N. Masciocchi, S. Galli, A. Sironi, J. Am. Chem. Soc. 126 (2004) 3014–3015;
A. Cingolani, S. Galli, N. Masciocchi, L. Pandolfo, C. Pettinari, A. Sironi, J. Am. Chem. Soc. 127 (2005) 6144–6145;
J.A.R. Navarro, E. Barea, J.M. Salas, C.O. Ania, J.B. Parra, N. Masciocchi, S. Galli, A. Sironi, J. Am. Chem. Soc. 130 (2008) 3978–3984.
[10] A. Maspero, S. Galli, V. Colombo, G. Peli, N. Masciocchi, S. Stagni, E. Barea, J.A.R. Navarro, Inorg. Chim. Acta 362 (2009) 4340–4346.
[11] S. Galli, N. Masciocchi, V. Colombo, A. Maspero, G. Palmisano, F.J. López-Garzón, M. Domingo-García, I. Fernández-Morales, E. Barea, J.A.R. Navarro, submitted.
[12] S. Galli, N. Masciocchi, G. Tagliabue, A. Sironi, J.A.R. Navarro, J.M. Salas, L. Mendez-Liñan, M. Domingo, M. Perez-Mendoza, E. Barea, Chem. Eur. J. 14 (2008) 9890–9901 and references therein.
[13] E.H.L. Falcao, Naraso, R.K. Feller, G. Wu, F. Wudl, A.K. Cheetam, Inorg. Chem. 47 (2008) 8336–8342.
[14] With the unique exception of the silver derivative **2**.
[15] A.R. Millward, O.M. Yaghi, J. Am. Chem. Soc. 127 (2005) 17998–17999.
[16] With other metal ions [Ni(II), Cd(II), Hg(II), Fe(II)], only intractable amorphous materials were obtained, which will not be discussed further.
[17] J.R. Johnson, D.H. Rotenberg, R. Ketcham, J. Am. Chem. Soc. 92 (1970) 4046–4050.
[18] J. Yamada, T. Sugimoto (Eds.), TTF Chemistry. Fundamentals and Applications of Tetrathiafulvalene, Germany and Kodansha Scientific Ltd., Tokyo, Japan, 2004 Springer Verlag, Berlin.
[19] P. Wagner, M. Kubicki, Acta Crystallogr. C59 (2003) o91–o92.
[20] P.M. Zorkii, T.V. Timofeeva, A.P. Polishchuk, Russ. Chem. Rev. 58 (1989) 1119–1144;
W. Helfrich, J. Phys. Colloq 40 (1979) C3-105–C3-114.
[21] R.D. Shannon, C.T. Prewitt, Acta Crystallogr. B25 (1969) 925–945.
[22] A. Bencini, M. Casarin, D. Forrer, L. Franco, F. Garau, N. Masciocchi, L. Pandolfo, C. Pettinari, M. Ruzzi, A. Vittadini, Inorg. Chem. 48 (2009) 4044–4451.
[23] E. Barea, G. Tagliabue, W.-G. Wang, M.J. Perez-Mendoza, L. Mendez-Liñan, F.J. Lopez-Garzon, S. Galli, N. Masciocchi, J.A.R. Navarro, Chem. Eur. J. 16 (2010) 931–937.
[24] A. Coelho, J. Appl. Crystallogr. 36 (2003) 86–95.
[25] R. Topas, General Profile and Structure Analysis Software for Powder Diffraction Data. Bruker AXS, Karlsruhe, Germany, 2001.
[26] A. Coelho, J. Appl. Crystallogr. 33 (2000) 899–908.
[27] R. Bossio, S. Marcaccini, R. Pepino, T. Torroba, G. Valle, Synthesis (1987) 1138–1139.
[28] R.W. Cheary, A. Coelho, J. Appl. Crystallogr. 25 (1992) 109–121.
[29] A. March, Z. Kristallogr. 81 (1932) 285–297;
W.A. Dollase, J. Appl. Crystallogr. 19 (1986) 267–272.
[30] J.A. Zampese, R.F. Keene, P.J. Steel, A similar (*N*,*N*′) coordination mode for a pyridine-substituted thiazolo-thiazole has been observed in Cu and Ru dimers. Dalton Trans. (2004) 4124–4129.
[31] O. Kahn, Y. Pei, I. Journaux, in: D.W. Bruce, D. O'Hare (Eds.), Inorganic Materials, J. Whyley, Chichester, UK, 1992.